Structural interface between LRRK2 and 14-3-3 protein

Biochemical Journal (2017) **0** 1–14
DOI: 10.1042/BCJ20161078

PORTLAND PRESS

Research Article

Structural interface between LRRK2 and 14-3-3 protein

Loes M. Stevers[1], Rens M.J.M. de Vries[1], Richard G. Doveston[1], Lech-Gustav Milroy[1], Luc Brunsveld[1] and Christian Ottmann[1,2]

[1]Laboratory of Chemical Biology, Department of Biomedical Engineering and Institute for Complex Molecular Systems, Eindhoven University of Technology, PO Box 513, 5600 MB Eindhoven, The Netherlands and [2]Department of Chemistry, University of Duisburg-Essen, 45141 Essen, Germany

Correspondence: Christian Ottmann (c.ottmann@tue.nl)

Binding of 14-3-3 proteins to leucine-rich repeat protein kinase 2 (LRRK2) is known to be impaired by many Parkinson's disease (PD)-relevant mutations. Abrogation of this interaction is connected to enhanced LRRK2 kinase activity, which in turn is implicated in increased ubiquitination of LRRK2, accumulation of LRRK2 into inclusion bodies and reduction in neurite length. Hence, the interaction between 14-3-3 and LRRK2 is of significant interest as a possible drug target for the treatment of PD. However, LRRK2 possesses multiple sites that, upon phosphorylation, can bind to 14-3-3, thus rendering the interaction relatively complex. Using biochemical assays and crystal structures, we characterize the multivalent interaction between these two proteins.

Introduction

Parkinson's disease (PD) is the second most common neurodegenerative disorder with only limited therapeutic options. In the majority of cases, PD occurs sporadically and is strongly age-related. However, many genes have been linked to inherited forms of PD, bearing implications for possible treatments of the disease [1]. Here, autosomal dominant, missense mutations in the leucine-rich repeat protein kinase 2 (LRRK2) gene are the most common genetic predispositions for PD [2–4]. About 1–5% of familial and sporadic PD show mutations in LRRK2 and patients with these mutations display a clinically identical disease phenotype as those with idiopathic PD [5–7]. Pathogenic PD mutations (N1437H, R1441C/G/H, Y1699C, I2020T and G2019S) in LRRK2 result in increased kinase activity and the formation of cytoplasmic accumulations [8–12]. One of the most important protein interaction partners of LRRK2 are the 14-3-3 proteins [11,13–16]. The primary binding motifs for 14-3-3 in LRRK2 were identified to be around phosphorylated serines 910, 935 and 1444, but also serines at position 860, 955 and 973 have been reported to bind to 14-3-3 upon phosphorylation [8,11,13–15,17,18]. The phosphorylated serines pS910, pS935, pS955 and pS973 are located in the disordered loop between the ANK and LRR domain; pS860 is located in the ANK domain close to this loop and pS1444 is located farther away in the ROC domain (Figure 1A). Importantly, many pathogenic mutations in LRKK2 disrupt or weaken the interaction with 14-3-3, thus implying a role of this protein–protein interaction (PPI) in PD (Figure 1B) [11,14–15]. Accordingly, 14-3-3 binding has been shown to regulate cytoplasmic distribution [13], to protect from dephosphorylation [15] and to be involved in extracellular secretion of LRRK2 [16]. Dephosphorylation of LRRK2 and consequent abrogation of 14-3-3 binding were recently reported to enhance ubiquitination of LRRK2 [17]. This enhanced degradation of LRRK2 could be involved in detrimental loss-of-function phenotypes found in peripheral tissues of LRRK2 kinase-inactive mutants [18] and also may have important consequences for pharmacological interventions on LRRK2 [19]. Furthermore, the group of Yacoubian showed that overexpression of 14-3-3 reversed shortening of neurites harboring the G2019S mutant of LRRK2 while, conversely, disruption of 14-3-3 functions by a peptide inhibitor further reduced neurite length in G2019S–LRRK2 cultures [20].

Received: 11 December 2016
Revised: 9 February 2017
Accepted: 14 February 2017

Accepted Manuscript online: 15 February 2017
Version of Record published: 0 Month 2017

Biochemical Journal (2017) **0** 1–14
DOI: 10.1042/BCJ20161078

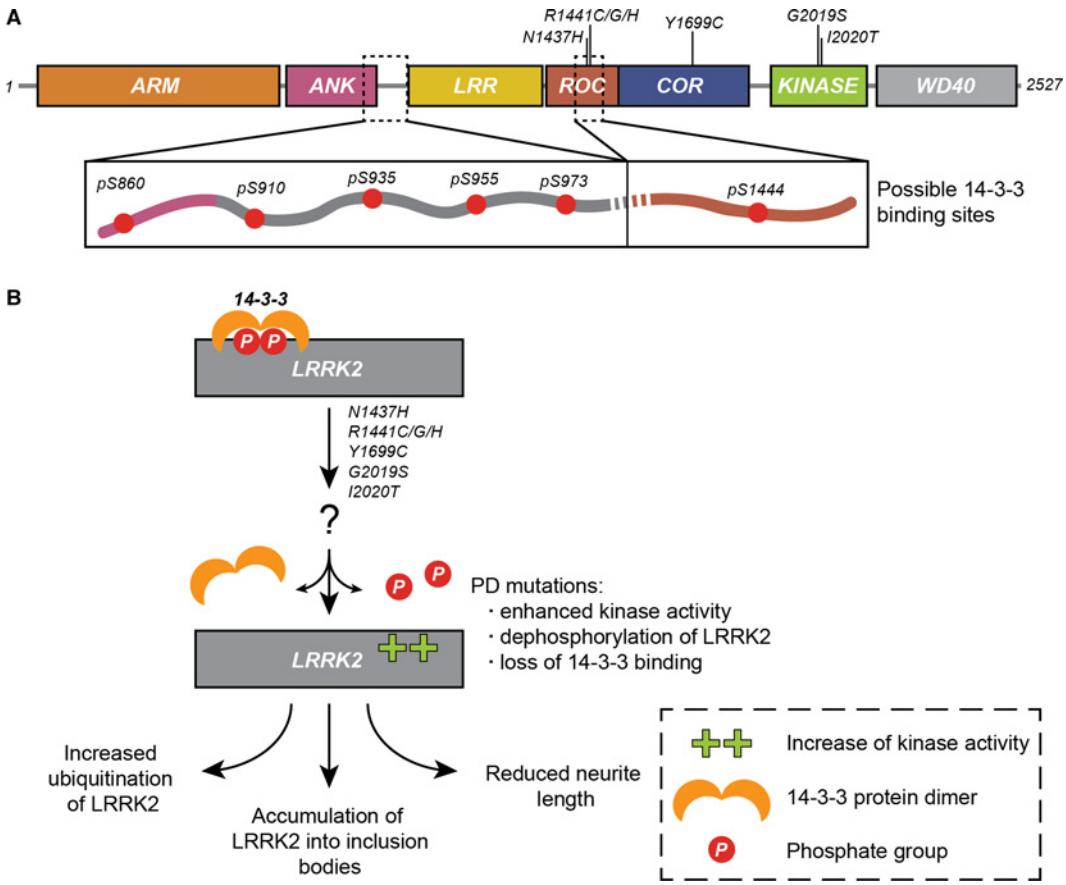

Figure 1. (**A**) Schematic overview of the LRRK2 protein domains (ARM, Armadillo; ANK, Ankyrin; LRR, Leucine-Rich Repeats; ROC, Ras of complex proteins; COR, C-terminal of ROC; Kinase; WD40), with the location of pathogenic PD mutations and a close-up of the location of the different potential 14-3-3-binding sites. (**B**) A cartoon view of 14-3-3 binding to phosphorylated LRRK2. Pathogenic PD mutations in LRRK2 lead to enhanced kinase activity, dephosphorylation of LRRK2 and the loss of 14-3-3 binding, resulting in increased ubiquitination of LRRK2, accumulation of LRRK2 into inclusion bodies and reduced neurite lengths.

To explain the positive effect of 14-3-3 binding toward PD, the group of Herberg proposed a model in which LRRK2 kinase activity is controlled by a conformational change driving the kinase into an inactive state, which is stabilized by 14-3-3 binding simultaneously to pS910 and pS1444 [11]. Interestingly, three clinically

Table 1 Amino acid sequence of peptides coding for six singly phosphorylated 14-3-3-binding sites in the LRRK2 protein

LRRK2pS1444 was extended (ex) with the natural sequence to improve solubility.

Peptide	Sequence
LRRK2pS860	E G T A S G **pS** D G N F S E
LRRK2pS910	V K K K S N **pS** I S V G E F
LRRK2pS935	L Q R H S N **pS** L G P I F D
LRRK2pS955	K R K I L S **pS** D D S L R S
LRRK2pS973	H M R H S D **pS** I S S L A S
LRRK2pS1444(ex)	I K A R A S **pS** S P V I L V (G T H L D)

Biochemical Journal (2017) **0** 1–14
DOI: 10.1042/BCJ20161078

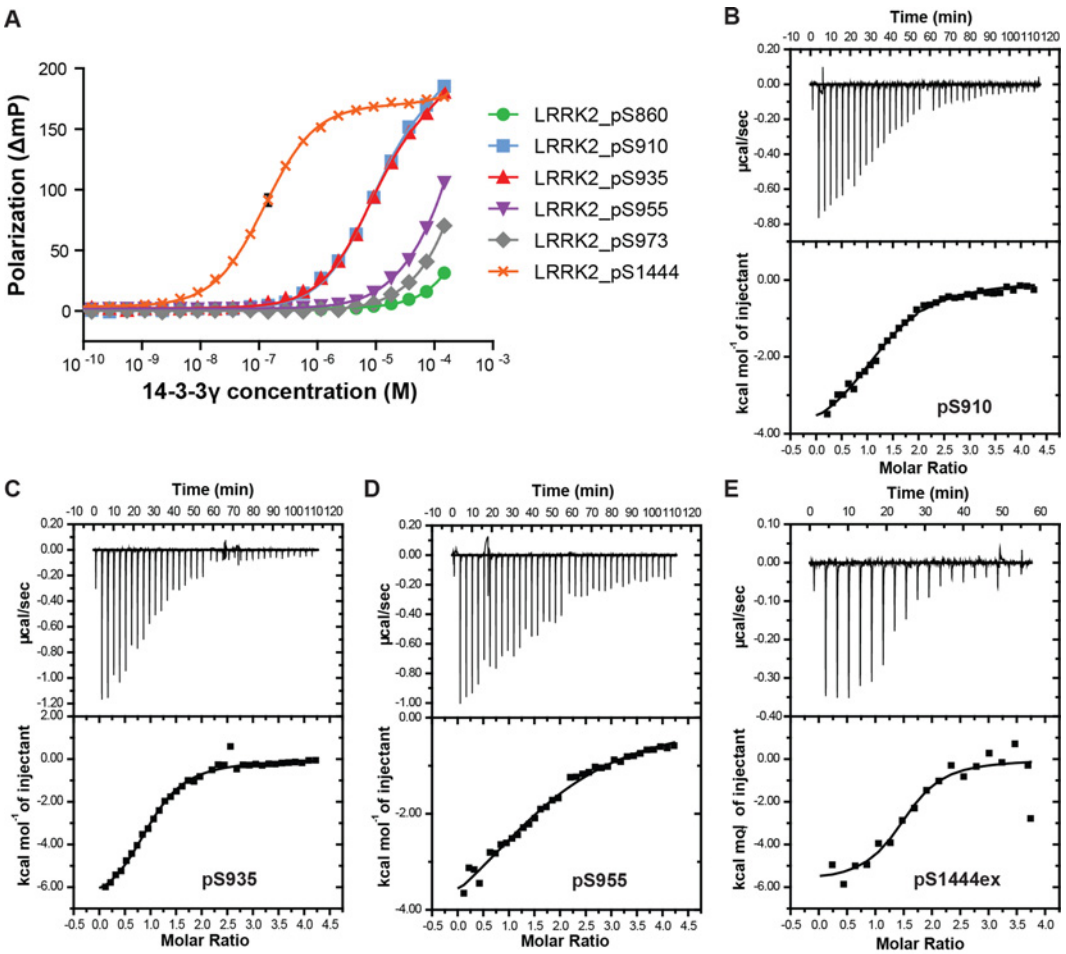

F

	Kd from FP (RT)	Kd from ITC (37 °C)
LRRK2_pS860	*n.d.*	*n.d.*
LRRK2_pS910	8.34 ±0.27 µM	28.5 ±2.8 µM
LRRK2_pS935	7.75 ±0.21 µM	16.9 ±2.3 µM
LRRK2_pS955	50.8 ±12.1 µM	93.5 ±13.8 µM
LRRK2_pS973	63.9 ±37.5 µM	*n.d.*
LRRK2_pS1444(ex)	0.125 ±0.003 µM	1.32 ±0.96 µM

Figure 2. Binding between six singly phosphorylated peptides representing segments of the LRRK2 protein (sequences are depicted in Table 1), and 14-3-3γ.

(**A**) FP assay of FITC-labeled peptides with 14-3-3γ. Background polarization was subtracted from all values. Mean of three experiments; SD error bars are presented when bigger than the data point symbols. (**B**–**E**) ITC results of the binding of the six peptides to 14-3-3γ. (**F**) Overview of the K_ds of the binding between the peptides and 14-3-3 based on FP and ITC assays.

observed mutations can be found — R1441C, R1441G and R1441H — that impair 14-3-3 binding by reducing phosphorylation on S1444 [11], but also possibly by a direct steric effect.

The 14-3-3 class of adapter proteins interacts with several hundred protein partners, of which many are involved in human disease [21–23]. Overall, the activity of 14-3-3 proteins is recognized as neuroprotective [24], for example by preventing neurofilament aggregation in amyotrophic lateral sclerosis [25]. Of high importance for chemical biology applications and potential drug discovery, small-molecule modulation of 14-3-3 PPIs has been shown by employing natural products [26,27], peptide derivatives [28,29], synthetic molecules [30,31] and supramolecular ligands [32,33]. For example, the natural product Cotylenin stabilizes the

Biochemical Journal (2017) 0 1–14
DOI: 10.1042/BCJ20161078

Table 2 Amino acid sequence of peptides coding for six doubly phosphorylated 14-3-3-binding sites in the LRRK2 protein

Peptides containing the pS1444 site were connected with a glycine/serine linker instead of the natural sequence.

Peptide	Sequence
LRRK2pS860pS910	E G T A S G **pS** D G N F S E G S G G G S G V K K K S N **pS** I S V G E F
LRRK2pS910pS935	V K K K S N **pS** I S V G E F Y R D A V L Q R C S P N L Q R H S N **pS** L G P I F D
LRRK2pS935pS955	L Q R H S N **pS** L G P I F D H E D L L K R K R K I L S **pS** D D S L R S
LRRK2pS955pS973	K R K I L S **pS** D D S L R S S K L Q S H M R H S D **pS** I S S L A S
LRRK2pS910pS1444	V K K K S N **pS** I S V G E F G S G G G S G I K A R A S **pS** S P V I L V G T H L D
LRRK2pS935pS1444	L Q R H S N **pS** L G P I F D G S G G G S G I K A R A S **pS** S P V I L V G T H L D

inhibitory binding of 14-3-3 to the protein kinase C-Raf and displays antitumor activity [27,34]. Given that (i) 14-3-3 binding to LRRK2 is impaired by many PD-relevant mutations [13–15], (ii) LRRK2 kinase activity is enhanced in PD [35] and (iii) this kinase activity is reduced upon binding to 14-3-3 [11], a possible and yet unaddressed strategy for treating PD could be small-molecule stabilization of the LRRK2/14-3-3 interaction. Here, we present the crystal structure of 14-3-3 in complex with the binding motifs of LRRK2 surrounding pS910 and pS935, and show how the different combinations of these two sites and pS1444 significantly enhance the binding strength of 14-3-3, indicating the importance of multivalency for LRRK2 regulation by 14-3-3 proteins. Finally, we discuss the possibility for small-molecule stabilization of the LRRK2/14-3-3 interaction as a potential approach for therapeutic modulation of LRRK2 activity in PD.

Materials and methods

Peptide synthesis

All peptides were synthesized via Fmoc solid-phase peptide synthesis making use of an Intavis MultiPep RSi peptide synthesizer. The singly phosphorylated peptides were synthesized on Rink amide resin (Novabiochem; 0.59 mmol/g loading) and the doubly phosphorylated peptides were synthesized on TentaGel R RAM resin (Rapp Polymere; 0.18 mmol/g). To increase the peptide synthesis yields, pseudoproline dipeptide residues [Fmoc-Ile-Ser(psiMe,Mepro)-OH, Fmoc-Asp(OtBu)-Ser(psiMe,Mepro)-OH and Fmoc-Leu-Ser(psiMe,Mepro)-OH, Novabiochem] were incorporated in the synthesis of the longer, doubly phosphorylated peptides. The peptides used for isothermal titration calorimetry (ITC) and crystallization were acetylated before deprotection and cleavage of the resin. The peptides used in the fluorescence polarization (FP) assay were labeled via an Fmoc-O1pen-OH linker (Iris Biotech GmbH) with fluorescein isothiocyanate (FITC; Sigma–Aldrich). The peptides were purified using a preparative LC–MS system that consisted of an LCQ Deca XP Max (Thermo Finnigan) ion-trap mass spectrometer equipped with a Surveyor autosampler and a Surveyor photodiode detector array detector (Thermo Finnigan). Solvents were pumped using a high-pressure gradient system using two LC-8A pumps (Shimadzu) for the preparative system and a two LC-20AD pumps (Shimadzu) for the analytical system. The crude mixture was purified on a reverse-phase C18 column (Atlantis T3 prep OBD, 5 μm, 150 × 19 mm, Waters) using a flow of 20 ml/ min and linear acetonitrile gradient in water with 0.1% v/v trifluoroacetic acid. Fractions with the correct mass were collected using a PrepFC fraction collector (Gilson, Inc.).

14-3-3 Expression

His_6-tagged 14-3-3 proteins (full-length and ΔC) were expressed in NiCo21(DE3)-competent cells with a pPROEX HTb plasmid and purified using Ni^{2+}-affinity chromatography. The ΔC variant meant for crystallization was treated with TEV protease to cleave off the His_6-tag, followed by a second Ni^{2+}-affinity column and size-exclusion chromatography. The proteins were dialyzed against FP, ICT or crystallization buffers before usage (recipes described below).

FP assay

The FITC-labeled peptides were dissolved in FP buffer [10 mM HEPES (pH 7.4), 150 mM NaCl, 0.1% Tween 20 and 1 mg/ml BSA) to a final concentration of 100 nM (singly phosphorylated peptides) or 5 nM (doubly

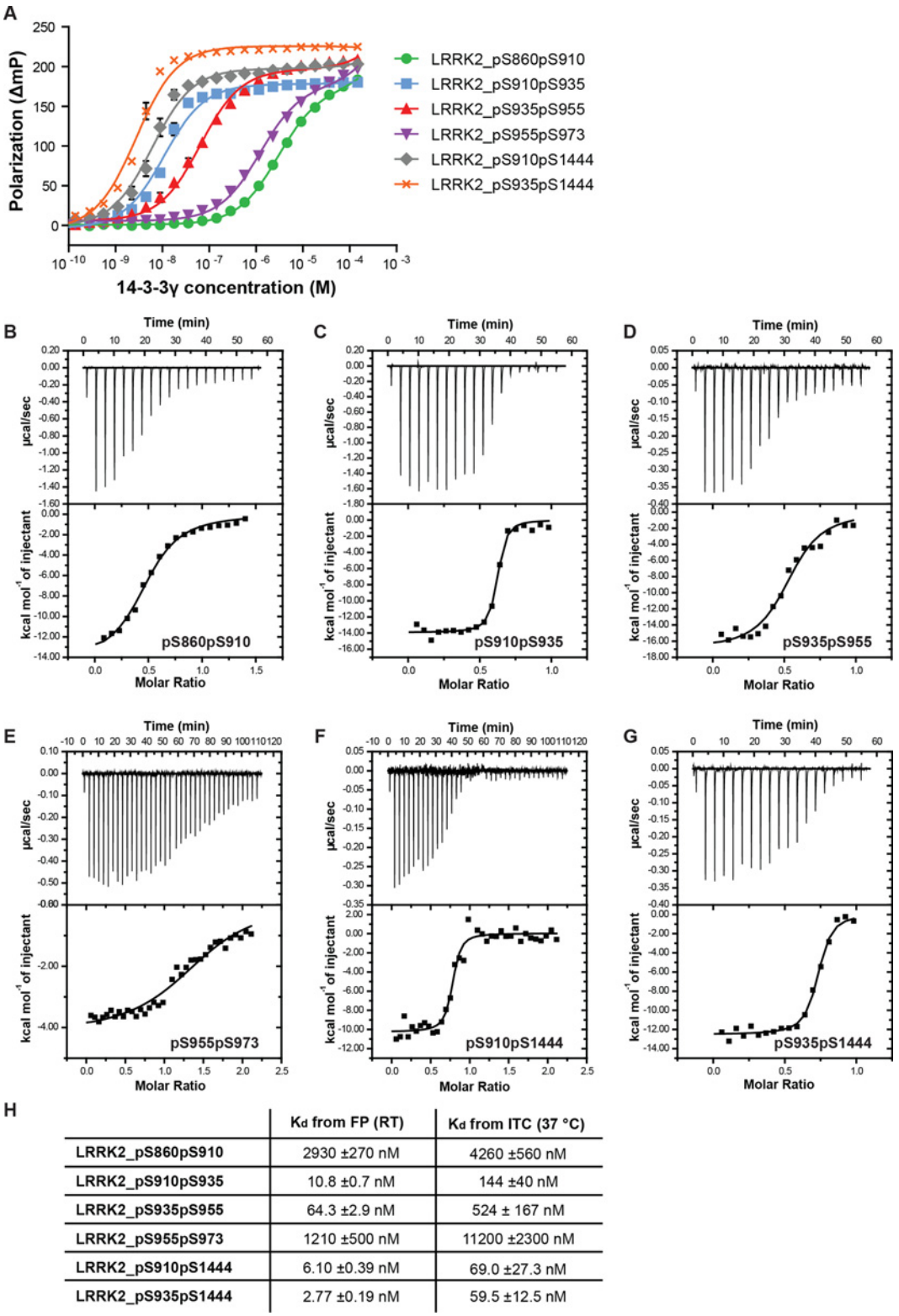

H

	Kd from FP (RT)	Kd from ITC (37 °C)
LRRK2_pS860pS910	2930 ±270 nM	4260 ±560 nM
LRRK2_pS910pS935	10.8 ±0.7 nM	144 ±40 nM
LRRK2_pS935pS955	64.3 ±2.9 nM	524 ± 167 nM
LRRK2_pS955pS973	1210 ±500 nM	11200 ±2300 nM
LRRK2_pS910pS1444	6.10 ±0.39 nM	69.0 ±27.3 nM
LRRK2_pS935pS1444	2.77 ±0.19 nM	59.5 ±12.5 nM

Figure 3. Binding between six doubly phosphorylated peptides representing segments of the LRRK2 protein (sequences are depicted in Table 2), and 14-3-3γ.

(**A**) FP assay of FITC-labeled peptides with 14-3-3γ. Background polarization was subtracted from all values. Mean of three experiments; SD error bars are presented when bigger than the data point symbols. (**B**–**E**) ITC results of the binding of the six peptides to 14-3-3γ. (**F**) An overview of the K_ds of the binding between the peptides and 14-3-3, based on the FP and the ITC assays.

Q17

Biochemical Journal (2017) 0 1–14
DOI: 10.1042/BCJ20161078

Table 3 Amino acid sequence of peptides coding for singly and doubly phosphorylated 14-3-3-binding sites in the LRRK2 protein with/without known PD causing mutations (R1441G/R1441C/R1441H) and phosphorylation on the S1444

Peptide	Sequence
LRRK2pS1444 (R1441G)	I K A G A S **pS** S P V I L V G T H L D
LRRK2pS1444 (R1441C)	I K A C A S **pS** S P V I L V G T H L D
LRRK2pS1444 (R1441H)	I K A H A S **pS** S P V I L V G T H L D
LRRK2S1444 (pS1444S)	I K A R A S S S P V I L V G T H L D
LRRK2S1444 (R1441G + pS1444S)	I K A G A S S S P V I L V G T H L D
LRRK2pS910pS1444 (R1441G)	V K K K S N **pS** I S V G E F G S G G G S G I K A G A S **pS** S P V I L V G T H L D
LRRK2pS910S1444 (pS1444S)	V K K K S N **pS** I S V G E F G S G G G S G I K A R A S S S P V I L V G T H L D
LRRK2_pS910S1444 (R1441G + pS1444S)	V K K K S N **pS** I S V G E F G S G G G S G I K A G A S S S P V I L V G T H L D

phosphorylated peptides). In these solutions, two times dilution series of 14-3-3 were made in Corning Black Round Bottom 384-well plates and their polarization was measured with a Tecan Infinite F500 plate reader (ex. = 485 nm and em. = 535 nm). The mean of three experiments is shown with SD error bars.

Isothermal titration calorimetry

The ITC measurements were performed with the Malvern MicroCal iTC$_{200}$. The protein and peptides were dissolved in ITC buffer [25 mM HEPES (pH 7.4), 100 mM NaCl, 10 mM $MgCl_2$ and 0.5 mM TCEP]. One or two times 18 titrations of 2 μl were performed at 37°C (reference power: 5 μCal/s, initial delay: 60 s, stirring speed: 750 rpm and spacing: 180 s). In case of two titration series, the data were merged with the ConCat32 software.

Crystallography

The 14-3-3σ protein was C-terminally truncated after T231 to enhance crystallization (14-3-3σΔC). The 14-3-3 protein and peptide were dissolved in crystallization buffer [25 mM HEPES, 0.1 M NaCl and 2 mM DTT (pH 7.4)] and mixed in a 1:1 stoichiometry with a final protein concentration of 10 mg/ml. This peptide–protein mixture was set up for sitting-drop crystallization in a home-made crystallization liquor [0.095 M HEPES, 0.19 M $CaCl_2$, 26% (v/v) PEG 400, 5% (v/v) glycerol (pH 7.3)]. Crystals were fished out after 13 days of incubation at 4°C and flash-cooled in liquid nitrogen. Diffraction data were collected at the X06SA/PXI beamline (Swiss Light Source, Villigen, Switzerland).

Results

Interaction of 14-3-3 with phosphorylated peptides comprising LRRK2 phosphorylation sites

To quantify the binding affinities of the 14-3-3 binding sites in LRRK2 reported previously [11,13,14], we synthesized peptides derived from LRRK2 and comprising the sequences around the phosphorylation sites Ser860, Ser910, Ser935, Ser955, Ser973 and Ser1444 (Table 1). For direct binding measurements to 14-3-3γ, these peptides were labeled with FITC and used in an FP assay. All peptides showed binding to 14-3-3γ albeit with marked differences in affinity (Figure 2A,F). LRRK2pS1444 exhibited the strongest binding affinity to 14-3-3γ with a K_d of 0.125 ± 0.003 μM, which is close to the K_d earlier reported by the group of Herberg (0.216 μM) [11]. LRRK2pS910 and LRRK2pS935 both bound around a 100-fold weaker (K_ds of 8.34 ± 0.27 and 7.75 ± 0.21 μM, respectively), which is in the case of LRRK2pS910 slightly weaker than reported by others (K_d of 661 ± 121 nM), however, significantly stronger for LRRK2pS935, where no binding of a synthetic phosphopeptide surrounding this site was shown [11]. The three weakest binders were LRRK2pS860, LRRK2pS955 and LRRK2pS973, of which the binding curves were not complete enough to determine their affinities for 14-3-3γ. To corroborate and further quantify the interaction of these synthetic LRRK2 peptides with a second, independent method, unlabeled

Biochemical Journal (2017) **0** 1–14
DOI: 10.1042/BCJ20161078

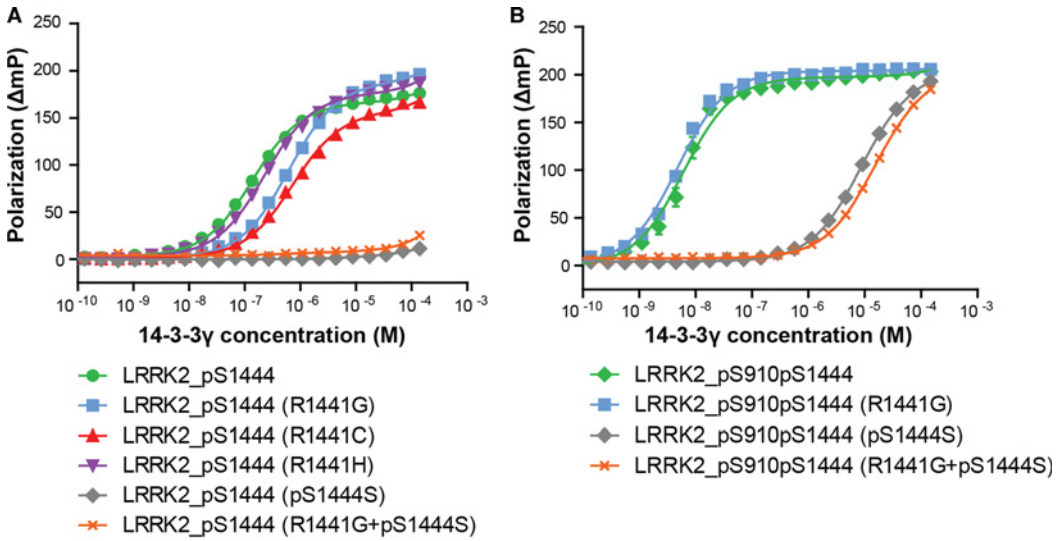

C

	Kd short peptide	Kd long peptide
Wild type	140 ±3 nM	6.10 ±0.39 nM
R1441G	617 ±13 nM	4.76 ±0.25 nM
R1441C	727 ±21 nM	*X*
R1441H	228 ±6 nM	*X*
pS1444S	*n.d.*	8320 ±260 nM
R1441G + pS1444S	*n.d.*	14400 ±700 nM

Figure 4. Binding between peptides representing segments of the LRRK2 protein, with or without PD-associated mutations (sequences are depicted in Table 3), and 14-3-3γ.

(**A**) FP assay of FITC-labeled peptides with 14-3-3γ. Background polarization was subtracted from all values. Mean of three experiments; SD error bars are presented when bigger than the data point symbols. (**B**) FP assay of FITC-labeled peptides with 14-3-3γ. Background polarization was subtracted from all values. Mean of three experiments; SD error bars are presented when bigger than the data point symbols. (**C**) Overview of the binding affinities (K_d) of the peptides and 14-3-3γ, based on the FP assay.

versions thereof were tested via ITC for their binding to 14-3-3γ (Figure 2B–F). The calculated affinities from ITC showed the same trend in binding for the six peptides as the results from the FP measurements (Figure 2F).

Many 14-3-3 partner proteins display more than one phosphorylated 14-3-3 recognition motif and, for many them (PKC, C-Raf, CFTR, Gab2), it was shown that simultaneous binding of two of these motifs to one 14-3-3 dimer dramatically increases the affinity [26,36–38]. Since LRRK2 also displays several potential and verified 14-3-3 binding sites, we synthesized many peptides where two of these phosphorylation sites were combined (Table 2). These peptides showed a strong increase in binding affinity to 14-3-3γ, with some of the combinations displaying the lowest K_ds ever reported for 14-3-3-binding peptides (Figure 3). For example, the FP assay of the two peptides containing pS1444 showed a K_d of 6.10 ± 0.39 nM for LRRK2pS910pS1444 and 2.77 ± 0.19 nM for LRRK2pS935pS1444 to 14-3-3γ. Also the binding of LRRK2pS910pS935 to 14-3-3γ could be fitted to a remarkably low K_d of 10.8 ± 0.7 nM as measured by FP (Figure 3E,H). A note has to be made that these values are measured close to the detection limit of the technique by the use of 5 nM of fluorescently labeled peptide, and it is thus possible that these peptides have even stronger binding affinities to 14-3-3γ. Also the other binding sites show an increase in affinity for 14-3-3γ by combining them with a second site (2.93 ± 0.27 μM for LRRK2pS860pS910, 64.3 ± 2.9 nM for LRRK2pS935pS955 and 1.21 ± 0.5 μM for LRRK2pS955pS973). It is remarkable that the addition of the barely measurable binding sites pS860 to pS910 still increases the affinity 2.8-fold. Again, these values were corroborated by ITC experiments, producing a comparable binding affinity trend for all peptides (Figure 3B–H). As observed in the FP assay, also with ITC the high-affinity peptides lay in the range of the detection limit of the technique.

Biochemical Journal (2017) **0** 1–14
DOI: 10.1042/BCJ20161078

Table 4 Crystallographic data table

	14-3-3σ/LRRK2_pS910 PDB ID: 5MYC	14-3-3σ/LRRK2_pS935 PDB ID: 5MY9
Data collection		
Wavelength (Å)	0.978620	0.978620
Resolution (Å)*	45.62–1.46 (1.54–1.46)	41.69–1.327 (1.375–1.327)
Space group	C 2 2 21	C 2 2 21
Cell parameters (Å)	$a = 82.52$, $b = 112.41$, $c = 62.69$	$a = 82.291$, $b = 112.030$, $c = 62.430$
$CC_{1/2}$ (%)*,†	100.0	99.9
R_{merge} (%)*,‡	0.082	0.124
R_{meas} (%)*,‡	0.085	0.129
Average $I/\sigma_{(I)}$*	21.96	14.99
Completeness (%)*	99.74	99.54
Number of unique reflections*	50 871	66 633
Redundancy*	8.2	12.4
Wilson B-factor (Å^2)	14.71	14.03
Mosaicity (°)	0.114	0.125
Refinement		
Number of protein/peptide/solvent atoms	1986/101/399	1993/32/358
R_{work}/R_{free} (%)	16.7/19.4	18.9/20.8
Number of reflections in the 'free' set	2543	3334
R.m.s. deviations from ideal values of bond lengths (Å)/bond angles (°)	0.006 / 0.76	0.005 / 0.75
Average B-factor (Å)	21.46	19.39
Ramachandran plot: favored/outlier residues (%)	98.52/0.00	98.45/0.00
Molprobity validation score	3.57	2.22

*Number in parentheses is for the highest resolution shell.
†$CC_{1/2}$ = Pearson's intra-dataset correlation coefficient, reported by SCALA (version 3.3.22).
‡Reported by SCALA (version 3.3.22).

Influence of mutations around LRRKpSer1444 on 14-3-3 binding

Whereas most PD-associated mutations in LRRK2 like G2019S, N1437H, Y1699C and I2020T are not found directly neighboring a 14-3-3-binding site, three mutations within the ROC domain (R1441C, R1441G and R1441H) have been shown to occur in a 14-3-3 recognition motif surrounding pS1444 [11]. Although it was reported that these mutations disturb the PKA recognition site and thus decrease phosphorylation of S1444 [14], we nonetheless wished to quantify the influence of these mutations on binding to 14-3-3 proteins, both in the context of the isolated LRRK2pS1444 site as well as in combination with one additional phosphorylation site, LRRK2pS910. The sequences of the peptides, we synthesized to this end can be found in Table 3. In line with earlier reports [14], we could not detect any interaction of the non-phosphorylated LRRK2S1444 (pS1444S) peptide with 14-3-3γ (Figure 4A) as measured via FP. When S1444 was phosphorylated, the R1441G, R1441C and R1444H mutations decreased the affinity of the peptide to 14-3-3 by a factor of around 5, 6 and 2, respectively (to 617 ± 13, 727 ± 21 and 228 ± 6 nM). This is in line with the idea that disturbance of the PKA recognition motif rather than a direct effect on 14-3-3 binding is largely responsible for the PD-related effect of this mutation.

Since LRRK2 can bind to 14-3-3 via multiple sites, we studied the effect of both the abrogation of phosphorylation at S1444 and the mutation R1441G in the context of a construct that displayed the phosphorylation of S910. Whereas the doubly phosphorylated peptide LRRK2pS910pS1444 bound to 14-3-3 with a K_d of around

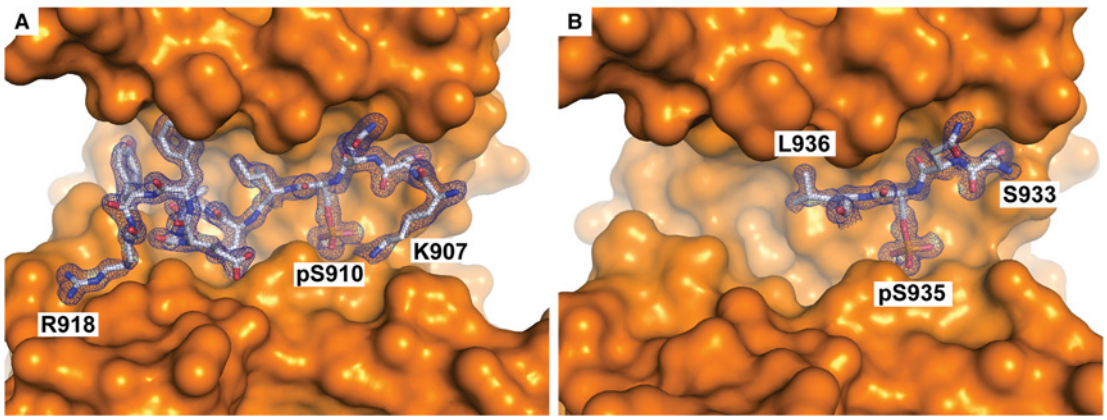

Figure 5. LRRK2pS910 and LRRK2pS935 binding to 14-3-3.

(**A**) Final $2F_O$–F_C electron density map (blue mesh, contoured at 2.5σ) of the LRRK2pS910 peptide (white sticks) binding to 14-3-3σ (orange surface). (**B**) Final $2F_O$–F_C electron density map (blue mesh, contoured at 2.5σ) of the LRRK2pS935 peptide (white sticks) binding to 14-3-3σ (orange surface).

5 nM (Figure 3), the affinity dropped by more than 1000-fold to 8.32 ± 0.26 μM when S1444 was not phosphorylated and to 14.4 ± 0.70 μM when, additionally, the R1441G mutation was present (Figure 4). These binding affinities are comparable with the shorter singly phosphorylated peptide LRRK2pS910, which bound with a K_d of 8.34 ± 0.27 μM, which suggests that the unphosphorylated S1444 does not play a role in binding to 14-3-3 (Table 4).

Crystal structure of 14-3-3 in complex with LRRK2pS910pS935

The LRRK2pS910pS935 and LRRK2pS935 peptides were co-crystallized with 14-3-3σ and their structures were solved to a resolution of 1.46 and 1.33 Å, respectively (Figure 5). In these crystal structures, interpretable densities of 12 amino acids surrounding the pS910 site, and four amino acids surrounding the pS935 site were found (Figure 5C,D). The remaining residues of the flexible linker between the two sites and the termini of both peptides are not visible in the electron density. The structures show the typical 14-3-3 binding of the phosphorylated serines in the basic pockets of the 14-3-3 dimer, with electrostatic interactions between R129, R56 and K49 of the 14-3-3 protein and the phosphate group of the phosphoserine. A hydrogen bond between Y130 of 14-3-3 and the phosphoserine strengthens these interactions (Figure 6A,C).

At the pS910 site, the binding is mostly based on polar interactions between the peptide and the 14-3-3-binding groove, presented with dashed lines in Figure 6A. However, also a cluster of hydrophobic amino acid side chains of the peptide (I911, V913 and F916) is positioned in a hydrophobic pocket formed by F119, P167, I168, L174, L218, I219 and L222 at the end of the binding groove of 14-3-3 (Figure 6B). Interestingly, eight amino acids lying C-terminally of pS910 are visible in the binding groove of 14-3-3, spanning a distance of only 14 Å. This is achieved by the peptide forming a α-helix which decreases the distance it crosses, thus making the structure more compact.

At the pS935 site fewer amino acids could be determined from the electron density map in the 14-3-3-binding groove. Polar interactions are visible C-terminal to the phosphorylated serine, between S933 of the peptide and E182 of the 14-3-3 protein, and the peptide backbone establishes interactions with residues W230, N226 and N175 of the protein. However, this interaction is mostly based on hydrophobic contacts between L936 of the peptide and L174, L218, I219 and L222 of 14-3-3. Beyond residue L936, the peptide forms a 'kink' protruding out of the binding groove, which leaves the rest of the binding groove empty, creating a rim-of-the-interface pocket.

Structural comparison with other 14-3-3-binding motifs

In recent years many crystal structures of 14-3-3-binding motif complexes have been published. As of January 2017, binding motifs of two dozen 14-3-3 partner proteins are deposited in the PDB, among them many biomedically relevant proteins like CFTR, p53, CRaf, Exoenzyme S (ExoS), ERα and Histone H3 [26,39,27,37,40–43].

Biochemical Journal (2017) **0** 1–14
DOI: 10.1042/BCJ20161078

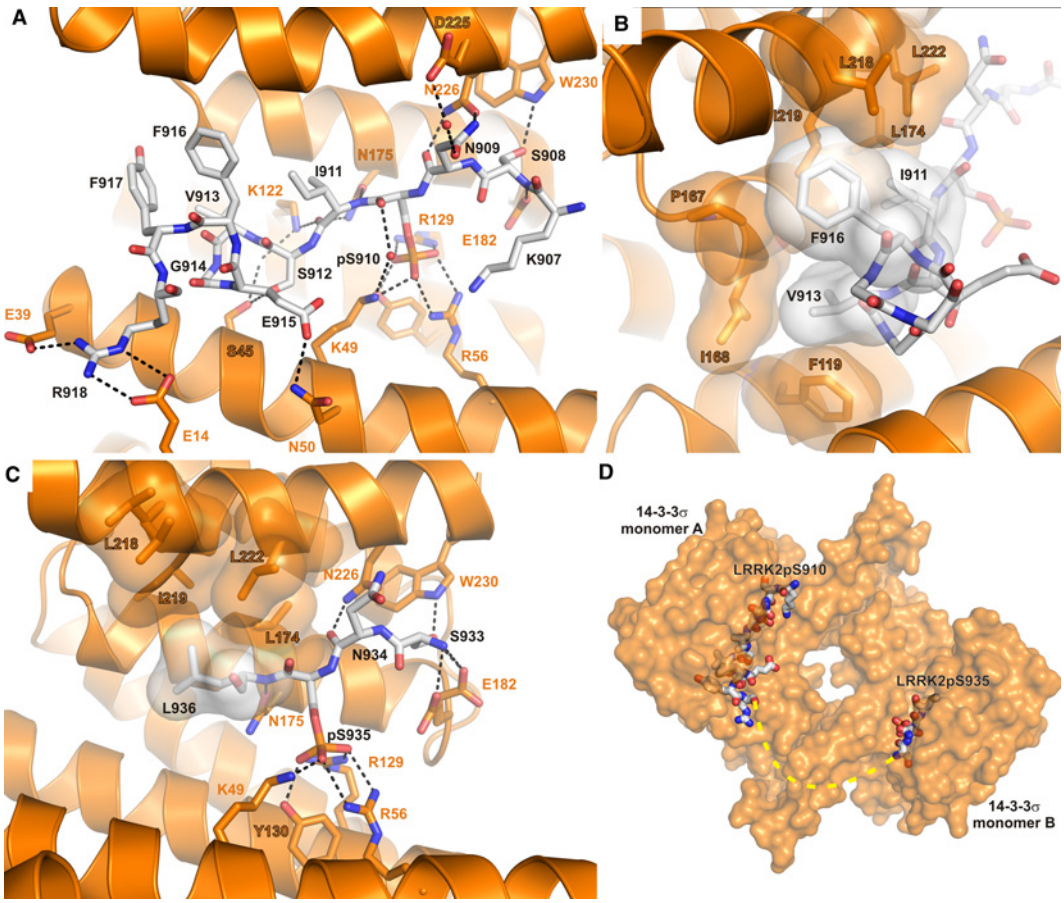

Figure 6. Protein–protein interaction interface between 14-3-3σ and LRRK2.

(**A**) Details of the LRRK2 peptide LRRK2pS910 (white sticks) binding to 14-3-3σ (orange cartoons and orange sticks). Polar interactions are depicted as black, dotted lines. (**B**) Hydrophobic interactions (semi-transparent surface) between LRRK2pS935 (white sticks) and 14-3-3σ (orange cartoon). (**C**) Detailed view of the LRRK2 peptide LRRK2pS910 (white sticks) binding to 14-3-3σ (orange cartoon and sticks) with polar interactions depicted as black, dotted lines and hydrophobic contacts shown as semi-transparent surface. (**D**) Surface representation of a 14-3-3σ dimer (orange) with bound LRRKpS910 (white sticks) by monomer A and LRRK2pS935 to monomer B.

Comparison of these structures with LRRKpS910 and LRRKpS935 reveals some interesting similarities. For example, the 14-3-3 interaction sites of CFTRpS768 and CRafpS259 span nearly the entire amphipathic binding channel, binding to 14-3-3 in an elongated fashion (Figure 7, upper panel). This is similar to the binding mode of LRRK2pS910 with the noticeable addition that residues 912–917 form a short α-helix. This is only the second time that a secondary structural element is observed in the primary interaction motif of a 14-3-3 partner protein. The first example is the phosphorylation-independent binding of the virulence factor ExoS from *Pseudomonas aeruginosa* [40,41]. ExoS binds in a phosphorylation-independent manner to 14-3-3, relying mostly on the hydrophobic interaction of four leucine residues with a hydrophobic patch in the amphipathic groove of 14-3-3. The second major difference from all phosphorylation-dependent 14-3-3 PPIs is the opposite orientation the ExoS peptide is co-ordinated by 14-3-3. Normally, 14-3-3 interactors are co-ordinated in an N- to C-terminal direction, starting from the phosphorylated residue binding basic pocket to the exit point of the amphipathic channel. In contrast, ExoS is co-ordinated from the C- to the N-terminus starting from the equivalent position in the basic pocket [41]. Nonetheless, the position of the α-helix formed by ExoS can be found at exactly the same position as in LRRK2pS910, indicating a predisposition of 14-3-3 proteins to accommodate this structural element in this part of the interaction interface with partner proteins.

Biochemical Journal (2017) **0** 1–14
DOI: 10.1042/BCJ20161078

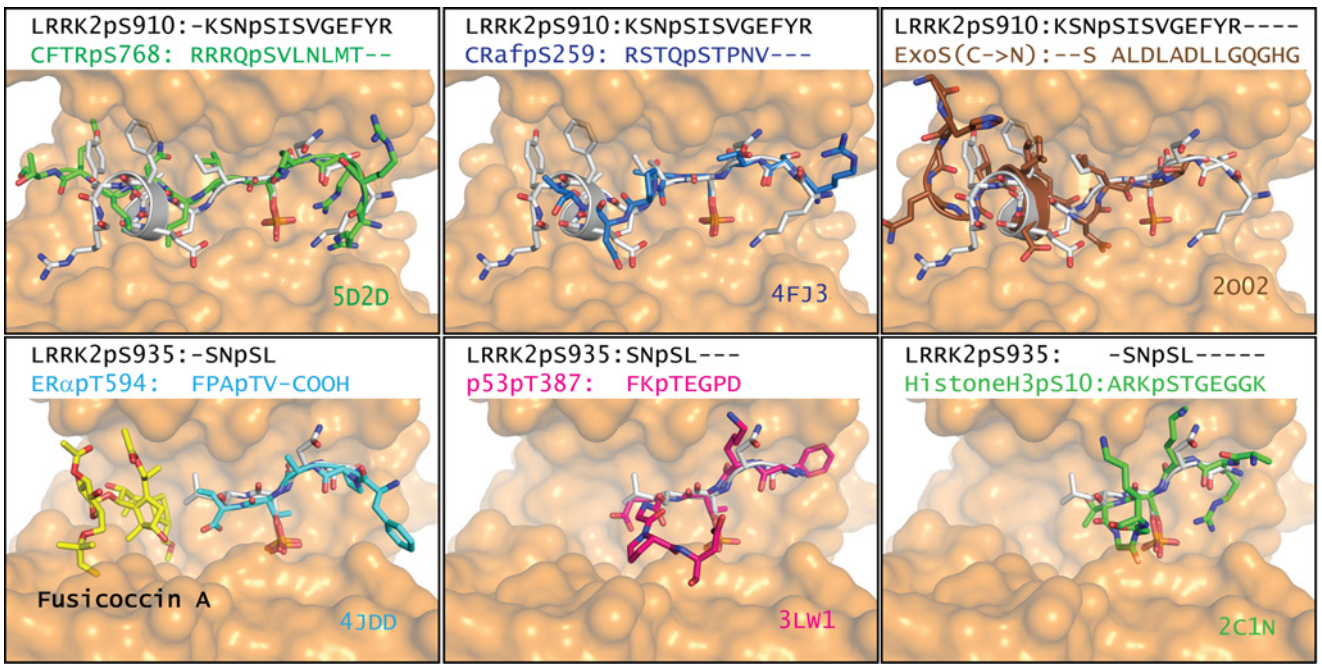

Figure 7. Sequence and three-dimensional comparison between LRRK2 binding to 14-3-3 and previously elucidated 14-3-3 protein complexes.
Upper row: 14-3-3 binding peptides that — similar to LRRK2pS910 — occupy nearly the entire length of the 14-3-3 binding channel. Lower row: 14-3-3 binding peptides that — similar to LRRK2pS935 — create an interface pocket that could accommodate a stabilizing molecule like Fusicoccin A. PDB codes of the structures used for creating the superimpositions are added.

Other interesting comparisons are those of the relatively limited interface of LRRK2pS935 with also short interacting sequences like those belonging to ERα, p53 and Histone H3. In all these structures, C-terminal from the phosphorylated serine or threonine residue the peptide chain either ends at position +1 (ERα) or makes a sharp turn to exit the binding groove of 14-3-3, leaving a well-defined, albeit open interface pocket. In principle, such a pocket can be targeted with a small molecule as we have shown with the tool compound Fusicoccin A in the case of the 14-3-3/ERα complex [42].

Discussion

The LRRK2 kinase is one of the most promising molecular targets for the treatment of PD [2,4,6]. As a protein kinase, the most obvious and established path forward is the development of active-site inhibitors [8]. Here, many promising developments have been reported recently showing the clinical potential of these molecules [44,45]. However, direct inhibition of the enzymatic activity of LRRK2 has been reported to also reduce LRRK2 levels in peripheral tissue [46–48]. The inhibitor-induced reduction in LRRK2 protein levels could lead to loss of function effects in peripheral tissues. In this context, a recent study testing two distinct LRRK2 inhibitors in non-human primates has shown that these kinase inhibitors induced abnormal cytoplasmic accumulation of secretory lysosome-related organelles in pneumocytes of the lung [49]. In another report, six different LRRK2 kinase inhibitors were used to show that LRRK2 kinase inhibition induces LRRK2 dephosphorylation and reduction in LRRK2 protein levels in mouse brain, lung and kidney overexpressing wild-type and G2019S, but not A2016T or K1906M LRRK2. This reduction in LRRK2 levels could be reversed by the proteasome inhibitor MG132, but not by lysosomal inhibition, while mRNA levels remained unaffected [50]. This potential side effect might represent a hurdle for LRRK2 inhibitor treatment in humans, and suggests that targeting LRRK2's kinase domain could be a 'double-edged sword' [19].

Recently, the class of 14-3-3 adapter proteins have been shown to play an important role as regulators of LRRK2 [13–18]. This highly conserved protein class is involved in a wide variety of physiological processes [51]. Both our FP and ITC measurements showed that the binding of LRRK2pS1444 to 14-3-3γ is significantly stronger than the other five reported 14-3-3 binding sites in LRRK2. Additionally, when this binding site is

Biochemical Journal (2017) 0 1–14
DOI: 10.1042/BCJ20161078

combined with another binding site (e.g. pS910 or pS935), the K_d is reduced to the low nM range. Nonetheless, it is important to realize that it has not been shown yet whether it is sterically possible for the LRRK2 protein to exist in a conformation whereby a 14-3-3 dimer can simultaneously bind to both pS1444 and the disordered loop between the ANK and LRR domains containing pS910 and pS935. A crystal structure or model of 14-3-3 with a larger section of LRRK2, containing at least the ROC, LRR and part of the ANK domain, could elucidate this. Furthermore, the doubly phosphorylated peptide LRRK2pS910pS935 demonstrated to have a higher affinity to 14-3-3γ than LRRK2pS1444 on its own. Additionally, the presence of the other three binding sites in the same, flexible region (pS860, pS955 and pS973) makes the effective concentration of 14-3-3-binding sites in this area relatively high. This hints toward an ultrasensitive response in the binding as has previously been shown in other PPIs with multisite phosphorylation (e.g. by Ferrell and Ha) [52]. However, further analysis is necessary to quantify the effect of multivalency in this example.

Importantly, dephosphorylation of S910 and S935 takes place prior to reduction in protein levels but mutation of these two sites to non-phosphorylatable alanines (S910A and S935A) had no influence on inhibitor-induced degradation of LRRK2 [50]. This interesting notion might hint at 14-3-3 dissociation from LRRK2 as a mechanistic prerequisite for LRRK2 degradation. If this would be the case, small-molecule stabilization of the 14-3-3/LRRK2 complex in order to inhibit kinase activity could simultaneously protect LRRK2 levels in peripheral organs from potentially harmful degradation. The biochemical and structural data of the interaction of 14-3-3 with LRRK2 presented here may be a good starting point for the identification and development of such a stabilizer. For example, the FP assays employing labeled synthetic phosphorylated peptides comprising the 14-3-3 recognition sites pS910, pS935 and pS1444 can be used to screen compound libraries to identify possible PPI stabilizers. The assay constructs of both 14-3-3 and LRRK2 are, in addition, suited for use in alternative assay formats like Homogenous Time-Resolved FRET (HTRF), AlphaScreen or Thermal-Shift Assay (TSA). Unfortunately, crystallization of 14-3-3/LRRK2pS1444 was not successful, but the crystal structures of LRRK2pS910 and LRRK2pS935 in complex with 14-3-3 form a sound structural basis for assessing 'ligandability' of these PPI interfaces. Here, especially the pS935 site displays a promising pocket at the rim of the interface where, in other 14-3-3 complexes, a very similar pocket can be targeted with the tool compound Fusicoccin A or its derivatives. In addition, stabilizing the physiological target complex of 14-3-3 with the plasma membrane H^+-ATPase PMA2 [53], Fusicoccins are also able to enhance binding of 14-3-3 to C-Raf [27], ERα [42], TASK3 [54], Gab2 [38] and CFTR [26]. However, we could not measure stabilization of LRRK2pS935 binding to 14-3-3 by Fusicoccin A (Supplementary Figure S1), which could be explained by a steric clash of residue Leu936 with the five-membered ring of Fusicoccin A. Nonetheless, visual inspection of the 14-3-3/LRRK2pS935 binary crystal structure suggests the possibility of finding an interface-binding molecule. While the success of *in silico* screening techniques as applied to PPI interfaces has not been proved yet, this type of investigation could provide valuable starting points. The use of crystals of the binary complexes for soaking of fragment cocktails represents a complementary experimental strategy.

In addition to the general relevance of 14-3-3 in neuroprotection [55] and in particular for the regulation of LRRK2, it is also of interest to note that the two other most prominent and best studied gene products associated with PD — the ubiquitin ligase Parkin and α-Synuclein (αSyn) — are binding partners of 14-3-3. Parkin dysfunction represents not only a predominant cause of familial Parkinsonism but also a formal risk factor for the more common, sporadic form of PD [56], and 14-3-3 proteins have been found to bind and modulate Parkin function [57]. αSyn was the first gene associated with familial PD and linked with many mutations as well as gene multiplications correlating with age of onset and severity of the disease [1]. A specific isoform of 14-3-3, 14-3-3η, has been shown to interact with aSyn, thereby reducing the cellular toxicity of aSyn [58]. Together with the findings that inhibition of LRRK2 might be a promising approach for PD therapy [44,45] and that 14-3-3 negatively regulates LRRK2 activity by binding to sites that are frequently mutated in familial forms of PD [11,13–15,20], it could be envisioned that small-molecule modulation of 14-3-3 binding to PD-related proteins may open up new possibilities for the development of therapeutic agents in PD.

Abbreviations

FITC, fluorescein isothiocyanate; FP, fluorescence polarization; ITC, isothermal titration calorimetry; LRRK2, leucine-rich repeat protein kinase 2; PD, Parkinson's disease; PPI, protein–protein interaction.

Author Contribution

Q11 **Funding**

This work was supported by the Collaborative Research Centre 1093, funded by the Deutsche Forschungsgemeinschaft (DFG), and the Netherlands Organization for Scientific Research via Gravity program **Q12** 024.001.035 and VICI grant [016.150.366].

Competing Interests

Q13 The Authors declare that there are no competing interests associated with the manuscript.

References

1 Kalinderi, K., Bostantjopoulou, S. and Fidani, L. (2016) The genetic background of Parkinson's disease: current progress and future prospects. *Acta Neurol. Scand.* **134**, 314–326 doi:10.1111/ane.12563
2 Zimprich, A., Biskup, S., Leitner, P., Lichtner, P., Farrer, M., Lincoln, S. et al. (2004) Mutations in LRRK2 cause autosomal-dominant parkinsonism with pleomorphic pathology. *Neuron* **44**, 601–607 doi:10.1016/j.neuron.2004.11.005
3 Paisán-Ruí´z, C., Jain, S., Evans, E.W., Gilks, W.P., Simón, J., van der Brug, M. et al. (2004) Cloning of the gene containing mutations that cause *PARK8*-linked Parkinson's disease. *Neuron* **44**, 595–600 doi:10.1016/j.neuron.2004.10.023
4 Di Fonzo, A., Rohé, C.F., Ferreira, J., Chien, H.F., Vacca, L., Stocchi, F. et al. (2005) A frequent LRRK2 gene mutation associated with autosomal dominant Parkinson's disease. *Lancet* **365**, 412–415 doi:10.1016/S0140-6736(05)17829-5
5 Healy, D.G., Falchi, M., O'Sullivan, S.S., Bonifati, V., Durr, A., Bressman, S. et al. (2008) Phenotype, genotype, and worldwide genetic penetrance of *LRRK2*-associated Parkinson's disease: a case–control study. *Lancet Neurol.* **7**, 583–590 doi:10.1016/S1474-4422(08)70117-0
6 Skipper, L., Li, Y., Bonnard, C., Pavanni, R., Yih, Y., Chua, E. et al. (2005) Comprehensive evaluation of common genetic variation within *LRRK2* reveals evidence for association with sporadic Parkinson's disease. *Hum. Mol. Genet.* **14**, 3549–3556 doi:10.1093/hmg/ddi376
7 Aasly, J.O., Toft, M., Fernandez-Mata, I., Kachergus, J., Hulihan, M., White, L.R. et al. (2005) Clinical features of LRRK2-associated Parkinson's disease in central Norway. *Ann. Neurol.* **57**, 762–765 doi:10.1002/ana.20456
8 Doggett, E.A., Zhao, J., Mork, C.N., Hu, D. and Nichols, R.J. (2012) Phosphorylation of LRRK2 serines 955 and 973 is disrupted by Parkinson's disease mutations and LRRK2 pharmacological inhibition. *J. Neurochem.* **120**, 37–45 doi:10.1111/j.1471-4159.2011.07537.x
9 Greene, I.D., Mastaglia, F., Meloni, B.P., West, K.A., Chieng, J., Mitchell, C.J. et al. (2014) Evidence that the LRRK2 ROC domain Parkinson's disease-associated mutants A1442P and R1441C exhibit increased intracellular degradation. *J. Neurosci. Res.* **92**, 506–516 doi:10.1002/jnr.23331
10 Ohta, E., Katayama, Y., Kawakami, F., Yamamoto, M., Tajima, K., Maekawa, T. et al. (2009) I(2020)T leucine-rich repeat kinase 2, the causative mutant molecule of familial Parkinson's disease, has a higher intracellular degradation rate than the wild-type molecule. *Biochem. Biophys. Res. Commun.* **390**, 710–715 doi:10.1016/j.bbrc.2009.10.034
11 Muda, K., Bertinetti, D., Gesellchen, F., Hermann, J.S., von Zweydorf, F., Geerlof, A. et al. (2014) Parkinson-related LRRK2 mutation R1441C/G/H impairs PKA phosphorylation of LRRK2 and disrupts its interaction with 14-3-3. *Proc. Natl Acad. Sci. U.S.A.* **111**, E34–E43 doi:10.1073/pnas.1312701111
12 Greggio, E. (2012) Role of LRRK2 kinase activity in the pathogenesis of Parkinson's disease. *Biochem. Soc. Trans.* **40**, 1058–1062 doi:10.1042/BST20120054
13 Dzamko, N., Deak, M., Hentati, F., Reith, A.D., Prescott, A.R., Alessi, D.R. et al. (2010) Inhibition of LRRK2 kinase activity leads to dephosphorylation of Ser^{910}/Ser^{935}, disruption of 14-3-3 binding and altered cytoplasmic localization. *Biochem. J.* **430**, 405–413 doi:10.1042/BJ20100784
14 Nichols, R.J., Dzamko, N., Morrice, N.A., Campbell, D.G., Deak, M., Ordureau, A. et al. (2010) 14-3-3 binding to LRRK2 is disrupted by multiple Parkinson's disease-associated mutations and regulates cytoplasmic localization. *Biochem. J.* **430**, 393–404 doi:10.1042/BJ20100483
15 Li, X., Wang, Q.J., Pan, N., Lee, S., Zhao, Y., Chait, B.T. et al. (2011) Phosphorylation-dependent 14-3-3 binding to LRRK2 is impaired by common mutations of familial Parkinson's disease. *PLoS ONE,* **6**, e17153 doi:10.1371/journal.pone.0017153
16 Fraser, K.B., Moehle, M.S., Daher, J.P.L., Webber, P.J., Williams, J.Y., Stewart, C.A. et al. (2013) LRRK2 secretion in exosomes is regulated by 14-3-3. *Hum. Mol. Genet.* **22**, 4988–5000 doi:10.1093/hmg/ddt346
17 Zhao, J., Molitor, T.P., Langston, J.W. and Nichols, R.J. (2015) LRRK2 dephosphorylation increases its ubiquitination. *Biochem. J.* **469**, 107–120 doi:10.1042/BJ20141305
18 Rudenko, I.N. and Cookson, M.R. (2010) 14-3-3 proteins are promising LRRK2 interactors. *Biochem. J.* **430**, e5–e6 doi:10.1042/BJ20101200
19 Melrose, H.L. (2015) LRRK2 and ubiquitination: implications for kinase inhibitor therapy. *Biochem. J.* **470**, e21–e24 doi:10.1042/BJ20150785
20 Lavalley, N.J., Slone, S.R., Ding, H., West, A.B. and Yacoubian, T.A. (2016) 14-3-3 proteins regulate mutant LRRK2 kinase activity and neurite shortening. *Hum. Mol. Genet.* **25**, 109–122 doi:10.1093/hmg/ddv453
21 Tinti, M., Madeira, F., Murugesan, G., Hoxhai, G., Toth, R. and Mackintosh, C. (2014) ANIA: ANnotation and integrated analysis of the 14-3-3 interactome. *Database (Oxford)*, **2014**, bat085 doi: 10.1093/database/bat085
22 Aghazadeh, Y. and Papadopoulos, V. (2016) The role of the 14-3-3 protein family in health, disease, and drug development. *Drug Discov. Today* **21**, 278–287 doi:10.1016/j.drudis.2015.09.012
23 Joo, Y., Schumacher, B., Landrieu, I., Bartel, M., Smet-Nocca, C., Jang, A. et al. (2015) Involvement of 14-3-3 in tubulin instability and impaired axon development is mediated by Tau. *FASEB J.* **29**, 4133–4144 doi:10.1096/fj.14-265009
24 Zha, J., Harada, H., Yang, E., Jockel, J. and Korsmeyer, S.J. (1996) Serine phosphorylation of death agonist BAD in response to survival factor results in binding to 14-3-3 not BCL-XL. *Cell* **87**, 619–628 doi:10.1016/S0092-8674(00)81382-3
25 Miao, L. Teng, J., Lin, J., Liao, X. and Chen, J. (2013) 14-3-3 proteins interact with neurofilament protein-L and regulate dynamic assembly of neurofilaments. *J. Cell Sci.* **126**, 427–436 doi:10.1242/jcs.105817
26 Stevers, L.M., Lam, C.V., Leysen, S.F.R., Meijer, F.A., van Scheppingen, D.S., de Vries, R.M. et al. (2016) Characterization and small-molecule stabilization of the multisite tandem binding between 14-3-3 and the R domain of CFTR. *Proc. Natl Acad. Sci.* **113**, E1152–E1161 doi:10.1073/pnas.1516631113

Biochemical Journal (2017) **0** 1–14
DOI: 10.1042/BCJ20161078

27 Molzan, M., Kasper, S., Röglin, L., Skwarczynska, M. Sassa, T., Inoue, T. et al. (2013) Stabilization of physical RAF/14-3-3 interaction by cotylenin A as treatment strategy for RAS mutant cancers. *ACS Chem. Biol.* **8**, 1869–1875 doi:10.1021/cb4003464

28 Glas, A., Bier, D., Hahne, G., Rademacher, C., Ottmann, C. and Grossmann, T.N. (2014) Constrained peptides with target-adapted cross-links as inhibitors of a pathogenic protein–protein interaction. *Angew. Chem. Int. Ed. Engl.* **53**, 2489–2493 doi:10.1002/anie.201310082

29 Milroy, L.-G., Bartel, M., Henen, M.A., Leysen, S., Adriaans, J.M.C., Brunsveld, L. et al. (2015) Stabilizer-Guided inhibition of protein–protein interactions. *Angew. Chem. Int. Ed. Engl.* **54**, 15720–15724 doi:10.1002/anie.201507976

30 Zhao, J., Du, Y., Horton, J.R., Upadhyay, A.K., Lou, B., Bai, Y. et al. (2011) Discovery and structural characterization of a small molecule 14-3-3 protein–protein interaction inhibitor. *Proc. Natl Acad. Sci. U.S.A.* **108**, 16212–16216 doi:10.1073/pnas.1100012108

31 Thiel, P., Röglin, L., Meissner, N., Hennig, S., Kohlbacher, O. and Ottmann, C. (2013) Virtual screening and experimental validation reveal novel small-molecule inhibitors of 14-3-3 protein–protein interactions. *Chem. Commun. (Camb.).* **49**, 8468 doi:10.1039/c3cc44612c

32 Bier, D., Rose, R., Bravo-Rodriguez, K., Bartel, M., Ramirez-Anguita, J.M., Dutt, S. et al. (2013) Molecular tweezers modulate 14-3-3 protein–protein interactions. *Nat. Chem.* **5**, 234–239 doi:10.1038/nchem.1570

33 Bier, D., Mittal, S., Sowislok, A., Briels, J., Heid, C., Bartel, M. et al. (2016) Molecular tweezers stabilize a disordered protein-protein interface. *Nat. Comm.* **Q14**

34 Kasukabe, T., Okabe-Kado, J., Kato, N., Honma, Y. and Kumakura, S. (2015) Cotylenin A and arsenic trioxide cooperatively suppress cell proliferation and cell invasion activity in human breast cancer cells. *Int. J. Oncol.* **46**, 841–848 **Q15**

35 West, A.B., Moore, D.J., Choi, C., Andrabi, S.A., Li, X., Dikeman, D. et al. (2006) Parkinson's disease-associated mutations in LRRK2 link enhanced GTP-binding and kinase activities to neuronal toxicity. *Hum. Mol. Genet.* **16**, 223–232 doi:10.1093/hmg/ddl471

36 Kostelecky, B., Saurin, A.T., Purkiss, A., Parker, P.J. and McDonald, N.Q. (2009) Recognition of an intra-chain tandem 14-3-3 binding site within PKCε. *EMBO Rep.* **10**, 983–989 doi:10.1038/embor.2009.150

37 Molzan, M. and Ottmann, C. (2012) Synergistic binding of the phosphorylated S233- and S259-binding sites of C-RAF to one 14-3-3ζ dimer. *J. Mol. Biol.* **423**, 486–495 doi:10.1016/j.jmb.2012.08.009

38 Bier, D., Bartel, M., Sies, K., Halbach, S., Higuchi, Y., Haranosono, Y. et al. (2016) Small-molecule stabilization of the 14-3-3/Gab2 protein–protein interaction (PPI) interface. *ChemMedChem* **11**, 911–918 doi:10.1002/cmdc.201500484

39 Schumacher, B., Mondry, J., Thiel, P., Weyand, M. and Ottmann, C. (2010) Structure of the p53 C-terminus bound to 14-3-3: implications for stabilization of the p53 tetramer. *FEBS Lett.* **584**, 1443–1448 doi:10.1016/j.febslet.2010.02.065

40 Fu, H., Coburn, J. and Collier, R.J. (1993) The eukaryotic host factor that activates Exoenzyme S of *Pseudomonas aeruginosa* is a member of the 14-3-3 protein family. *Proc. Natl Acad. Sci. U.S.A.* **90**, 2320–2324 doi:10.1073/pnas.90.6.2320

41 Ottmann, C., Yasmin, L., Weyand, M., Veesenmeyer, J.L., Diaz, M.H., Palmer, R.H. et al. (2007) Phosphorylation-independent interaction between 14-3-3 and Exoenzyme S: from structure to pathogenesis. *EMBO J.* **26**, 902–913 doi:10.1038/sj.emboj.7601530

42 De Vries-van Leeuwen, I.J., da Costa Pereira, D., Flach, K.D., Piersma, S.R., Haase, C., Bier, D. et al. (2013) Interaction of 14-3-3 proteins with the estrogen receptor alpha F domain provides a drug target interface. *Proc. Natl Acad. Sci. U.S.A.* **110**, 8894–8899 doi:10.1073/pnas.1220809110

43 Macdonald, N., Welburn, J.P.I., Noble, M.E.M., Nguyen, A., Yaffe, M.B., Clynes, D. et al. (2005) Molecular basis for the recognition of phosphorylated and phosphoacetylated histone h3 by 14-3-3. *Mol. Cell.* **20**, 199–211 doi:10.1016/j.molcel.2005.08.032

44 West, A.B. (2015) Ten years and counting: moving leucine-rich repeat kinase 2 inhibitors to the clinic. *Mov. Disord.* **30**, 180–189 doi:10.1002/mds.26075

45 Gilligan, P. (2015) Inhibitors of leucine-rich repeat kinase 2 (LRRK2): progress and promise for the treatment of Parkinson's disease. *Curr. Top. Med. Chem.* **15**, 927–938 doi:10.2174/1568026615101503282236 55

46 Herzig, M.C., Kolly, C., Persohn, E., Theil, D., Schweizer, T., Hafner, T. et al. (2011) LRRK2 protein levels are determined by kinase function and are crucial for kidney and lung homeostasis in mice. *Hum. Mol. Genet.* **20**, 4209–4223 doi:10.1093/hmg/ddr348

47 Lobbestael, E., Deman, S., De Wit, D., Taymans, J.M. and Baekelandt, V. (2015) LRRK2 kinase inhibition reduces endogenous LRRK2 protein levels in vivo. *Neurodegener. Dis.* **15**(Suppl. 1), 1186

48 Skibinski, G., Nakamura, K., Cookson, M.R. and Finkbeiner, S. (2014) Mutant LRRK2 toxicity in neurons depends on LRRK2 levels and synuclein but not kinase activity or inclusion bodies. *J. Neurosci.* **34**, 418–433 doi:10.1523/JNEUROSCI.2712-13.2014

49 Fuji, R.N., Flagella, M., Baca, M., Baptista, M.A., Brodbeck, J., Chan, B.K. et al. (2015) Effect of selective LRRK2 kinase inhibition on nonhuman primate lung. *Sci. Transl. Med.* **7**, 273ra215 doi:10.1126/scitranslmed.aaa3634

50 Lobbestael, E., Civiero, L., De Wit, T., Taymans, J.-M., Greggio, E. and Baekelandt, V. (2016) Pharmacological LRRK2 kinase inhibition induces LRRK2 protein destabilization and proteasomal degradation. *Sci. Rep.* **6**, 33897. doi:10.1038/srep33897

51 Fu, H., Subramanian, R.R. and Masters, S.C. (2000) 14-3-3 proteins: structure, function, and regulation. *Annu. Rev. Pharmacol. Toxicol.* **40**, 617–647 doi:10.1146/annurev.pharmtox.40.1.617

52 Ferrel, Jr, J.E., Ha, S.H. (2014) Ultrasensitivity part II: multisite phosphorylation, stoichiometric inhibitors, and positive feedback. *Trends Biochem. Sci.* **39**, 556–569 doi:10.1016/j.tibs.2014.09.003

53 Ottmann, C., Marco, S., Jaspert, N., Marcon, C., Schauer, N., Weyand, M. et al. (2007) Structure of a 14-3-3 coordinated hexamer of the plant plasma membrane H^+-ATPase by combining X-ray crystallography and electron cryomicroscopy. *Mol. Cell* **25**, 427–440 doi:10.1016/j.molcel.2006.12.017

54 Anders, C., Higuchi, Y., Koschinsky, K., Bartel, M., Schumacher, B., Thiel, P. et al. (2013) A semisynthetic fusicoccane stabilizes a protein–protein interaction and enhances the expression of K^+ channels at the cell surface. *Chem. Biol.* **20**, 583–593 doi:10.1016/j.chembiol.2013.03.015

55 Shimada, T., Fournier, A.E. and Yamagata, K. (2013) Neuroprotective function of 14-3-3 proteins in neurodegeneration. *Biomed. Res. Int.* **2013**, Article ID 564534 doi:10.1155/2013/564534

56 Zhang, C.W., Hang, L., Yao, T.P. and Lim, K.L. (2015) Parkin regulation and neurodegenerative disorders. *Front. Aging. Neurosci.* **7**, 248 doi:10.3389/fnagi.2015.00248

57 Sato, S., Chiba, T., Sakata, E., Kato, K., Mizuno, Y., Hattori, N. et al. (2006) 14-3-3η is a novel regulator of Parkin ubiquitin ligase. *EMBO J.* **25**, 211–221 doi:10.1038/sj.emboj.7600774

58 Plotegher, N., Kumar, D., Tessari, I., Brucale, M., Munari, F., Tosatto, L. et al. (2014) The chaperone-like protein 14-3-3η interacts with human α-synuclein aggregation intermediates rerouting the amyloidogenic pathway and reducing α-synuclein cellular toxicity. *Hum. Mol. Genet.* **23**, 5615–5629 doi:10.1093/hmg/ddu275